J Appl Electrochem (2009) 39:2439–2452
DOI 10.1007/s10800-009-9933-z

ORIGINAL PAPER

# AC impedance investigation of conductivity of automotive lubricants using two- and four-electrode electrochemical cells

**Vadim F. Lvovich · Matthew F. Smiechowski**

Received: 4 November 2008 / Accepted: 11 May 2009 / Published online: 28 May 2009
© Springer Science+Business Media B.V. 2009

**Abstract** Two- and four-electrode electrochemical cells were designed for characterization studies of highly resistive non-aqueous automotive lubricant using electrochemical impedance spectroscopy (EIS). The influence of internal configuration of the impedance analyzer, the media's temperature and properties, shielding of the cables, and the electrochemical cell geometry and arrangement on the impedance results were investigated. The most accurate EIS measurements can be made in the two-electrode configuration with active shields where a single arc at high frequencies and a complicated low frequency impedance feature were observed in complex impedance plots. When four-electrode cells were employed, the impedance load, geometry and positioning of voltage electrodes; finite resistance of the impedance analyzer; and capacitive coupling between the signal lines introduced two types of impedance measurement artifacts. A capacitive-resistive low frequency load was interpreted as a measurement artifact originating from geometry and positioning of voltage electrodes. The appearance of additional medium frequency load combining resistive, capacitive and inductive features is intrinsic to the measurement setup and is due to a combination of several instrumental and experimental factors resulting in a voltage divider effect.

**Keywords** Electrochemical impedance · Lubricants · Reference voltage electrodes · Four-electrode cell · Equivalent circuits

## 1 Introduction

Fully formulated lubricant can be viewed as a nonaqueous colloidal polymeric system with low, primarily ionic, electrical conductivity and corresponding solution impedances in excess of 1 MΩ even at elevated temperatures [1–3]. The dipolar nature of automotive lubricant components permits an investigation of their properties using Electrochemical Impedance Spectroscopy (EIS). EIS features huge experimental efficiency as it contains all necessary electrochemical information, the data quality and the system's stability can be checked by Kramers-Kronig transformation, and the results can be interpreted and modeled as equivalent circuits (EC) [4–6]. EIS presents an opportunity to resolve a complicated nonaqueous colloidal system both spatially and chemically, and to analyze specific parts of that system based on relaxation frequencies. The ac impedance technique is compatible with the harsh, low conductivity/high resistance, complex chemistry media of lubricants, polymers and colloids. The process of lubricant degradation is relatively slow, as it typically requires many weeks to significantly degrade a fully formulated automotive grade lubricant. Therefore it can be assumed that the system is stable over the course of a single EIS

Vadim F. Lvovich—ISE and ECS member.

V. F. Lvovich (✉)
Department of Biomedical Engineering (ND20), Lerner Research Institute, The Cleveland Clinic Foundation, 9500 Euclid Ave., Cleveland, OH 44195, USA
e-mail: vlvovich@ameritech.net

V. F. Lvovich
Department of Chemical Engineering, Case Western Reserve University, A.W. Smith Building, 10900 Euclid Ave., Cleveland, OH 44106, USA

M. F. Smiechowski
Guild Associates, Inc., 5750 Shier-Rings Rd., Dublin, OH 43016, USA

measurement, and the signal changes between fresh and aged lubricant are representative of chemical changes [7].

Our previous publications established an interpretation of physical and chemical characteristics of a typical lubricant using the linear [7, 8] and non-linear higher harmonic EIS analysis [9] for investigating the effects of oil oxidation; contamination with water [10], soot [11, 12] and fuel [13]; and development of various monitoring devices for lubricants' performance diagnostics [14, 15]. These studies were based on initial knowledge of chemical composition and physical properties of lubricants, and determining the response of various segments of the EIS spectrum to variations in the lubricants' ageing (degradation), chemical composition, electrochemical dc potential, temperature and electrode geometry in order to assess complex processes and decomposition pathways occurring both at the electrode-lubricant interface and in the bulk solution.

These studies resulted in the development of an equivalent circuit model for a typical lubricant taking into account relaxations related to bulk solution and interfacial processes. The low frequency impedance data was modeled as a parallel combination of a constant phase element ($CPE_{DL}$) representing double layer charging processes, charge transfer resistance ($R_{CT}$) of slowly discharging solution species, and a series combination of processes related to finite diffusion ($Z_{DIFF}$) and adsorption ($Z_{ADS}$) of surface-active lubricant additives [9]. The bulk solution region was represented by a series combination of at least two parallel R|C circuits [7] and was interpreted according to a "brick layer" impedance model of polycrystalline composite media composed of spheres of vastly different conductivities (where a more conductive phase is suspended inside less conductive additive/base oil matrix) [16]. The developed model is in good agreement with the general representation of polymeric and organic colloidal bulk solution structures as reported in publications based on impedance and dielectric studies [17].

The accurate measurement of lubricant bulk and interfacial impedance features is critical for evaluating lubricant properties and degradation rates [8, 18]. It is clear that solution conductivity and interfacial impedance measurements are influenced by both the employed technique and the cell geometry. It is generally acknowledged that accurate measurements can be made in a two-electrode configuration with shielded lead wires, where the influence of stray capacitance and lead inductance can be practically eliminated. But in EIS measurements, reference voltage electrodes are sometimes introduced for controlling the potential of a half-cell or voltage drop, and to measure the polarization of a working electrode. Standard electrochemistry methods can be employed to a two-, three- and four-electrode configuration to make accurate and sensitive electrochemical measurements. In this paper we review a possibility of applying multi-electrode electrochemical cells containing 1 working, 1 counter and 2 reference electrodes to impedance measurements in the highly resistive environment of a typical automotive lubricant.

In a *two-electrode cell*, one electrode serves as a combined working and reference electrode, and another electrode serves as a combined counter electrode and second reference electrode. The impedance is always measured between two reference electrodes, that is, the total measured impedance includes that of the counter electrode, the electrolyte solution and the working electrode. This type of electrode arrangement is typically used if it is impossible to position a reference electrode in the electrochemical cell, for example in the characterization of batteries, or when it is important to maintain a homogeneous current distribution, as in low conductivity media where an inhomogeneous current distribution can lead to measurement artifacts. We used this particular configuration in our previous studies [7–15].

In a two-electrode cell configuration, the current-generating electrodes also serve as voltage-measuring sensors. In highly resistive ionic solutions this often results in the interfacial polarization effects being predominant in the low-frequency impedance region. Under the AC field, a significant number of ions reach the electrode before reversal of polarity, which results in a charge build-up at the electrode interface, but no charge crosses the interface due to blocking. Polarization of electrodes is a problem in low conductivity media where there are only a few oxidizable or reducible polar species, which can eliminate polarization through charge transport on electrodes. In some cases, the interfacial polarization may result in the charged particles in the sensing zone far from the electrodes starting to move slowly because of the diminished electric field, and to appear to have lower electrophoretic mobility than they actually do [19]. The space charge diminishes the effective electric field in the bulk liquid, increases the measured bulk solution resistance ($R_{BULK}$), and affects the interfacial impedance region analyzed at low frequencies. We did not observe blocking behavior in our previous studies as adsorption and other effects dominate the low-frequency range and allow the charges to dissipate; however, some charge build-up effect on bulk solution resistance was reported [7].

It is generally perceived that using a *four-electrode cell* for impedance analysis offers an advantage over a two-electrode cell, because the measurement is free of contributions from the interfacial polarization and associated effects of surface charges build-up.

In a four-electrode cell two electrodes supply current to the cell and two additional voltage reference electrodes, connected through a high impedance device and placed between two current leads, are used to measure the potential directly in the cell. This way the contribution to the overall

measurement from contact impedances (with interfacial polarization being often a factor), lead resistances, and lead inductances of the current-generating electrodes are almost completely eliminated. Studies of applications of two-electrode and four-electrode electrochemical cells to Nafion membrane characterization [20, 21] reported a change in the characteristic of the measured low frequency impedance from a completely blocking interface for the two-electrode cell to an open-circuit transmission line for the four-electrode cell. Depending on particular geometry and positioning of the voltage electrodes, additional inductive and capacitive medium and low frequency impedance features were also reported.

Minimization of experimental current and voltage measurement error for a given sample should be achievable by choosing an electrode configuration that decreases total measured sample impedance ($Z_{SAMPLE}$), by increasing the current and voltage electrode active areas, and by minimizing the spacing between the voltage electrodes [22]. However, depending on the resulting electrode configuration, this solution may introduce additional errors due to creation of a strongly non-homogeneous electric field as a result of the insertion of large voltage electrode barriers to the current flow. In addition to that, an overall increase in the size of the voltage electrodes can lead to the introduction of an artifact related to their relative thickness and positioning. Expanding the surface area of the voltage electrodes generally implies the use of a thicker material, leading to a separate low frequency capacitive artifact [22].

An alternative method to reduce the measurement error is to increase the measured sample impedance and minimize the inhomogeneous electric field effects by increasing the gap between the voltage electrodes, decreasing the gap between the voltage and the current electrodes, and reducing the voltage electrodes geometrical sizes. These steps should result in minimizing the voltage electrodes' interference with the homogeneous electric field, lower parasitic currents, and potentially allow thinner electrodes with a corresponding decrease in the low frequency geometry and positioning-related artifact. Therefore, in order to ensure this contact impedance is minimized, electrodes with a small contact area to the sample, e.g. needles or rings, are recommended for the voltage electrodes. Studies of this configuration reported that four-electrode electrochemical cells containing thin wire or rod-like voltage electrodes produced more accurate estimations of bulk solution conductivity, than cells containing plate voltage electrodes with a large contact area [20]. It was also reported that the ionic resistance could be satisfactorily resolved from interfacial impedance only when the frequency is greater than 100 Hz [21]. However, this approach leads to higher interfacial impedance of the voltage electrodes in combination with the instrumental load [22, 23].

Contact between the sample and the electrodes may create an additional network with some interface impedances forming at all four electrodes and a parasitic current flowing through the voltage electrode pair [20]. The literature data presented a study on a Nafion membrane sample with the measured bulk solution resistances on the order of 1 kΩ. Data plots for four-electrode cells with small surface area voltage electrodes revealed a substantial medium frequency inductive loading, which adversely affected accuracy of conductivity measurements. Large surface area voltage electrodes showed less of the inductive interference, but produced an additional low frequency capacitive load. Quite surprisingly both of these low frequency effects were attributed by the authors to interfacial impedance effects, which are actually not measured in a four-electrode cell model [20].

Another consideration can also affect the selection of the cell arrangement and geometry. To achieve more accurate measurement, the voltage electrodes should be connected through a high impedance device so that negligible parasitic current flows across these interfaces. A combination of the parasitic current and the contact impedances creates a voltage drop, which further causes an error in the total measured output voltage of the system. To minimize the effects of this additional network one has to make sure that the voltage drop is very small against measured total output voltage. For this purpose a configuration consisting of large surface area voltage electrodes with a small separation between the voltage and current electrodes should be selected, which is exactly opposite of the configuration for thin wire or rod-like electrodes described above.

Further improvement in the impedance analysis using four-electrode cells is expected from minimizing the cables' loading capacitance using drive active shields, as was reported in a previous study of application of a four-electrode electrochemical cell to conductivity measurements in solid-state devices with bulk resistances in the low MΩ to low GΩ range [22, 23]. The effects of the system set-up and errors of measurements, such as bias currents to the amplifier inputs, cable capacity, coupling capacity between different leads, input impedance of the amplifier, loads of the electrodes, cable active shielding, current distribution across the solution, positioning of the electrodes and their shapes were studied. The paper concluded that generally accurate impedance measurements could be achieved by using a four-electrode cell only for samples with resistance less than 1 MΩ [23]. For samples with bulk resistance in excess of 1 MΩ the accurate impedance characterization becomes difficult and requires a careful analysis of several contributions. For example, small voltage electrodes can cause inductive interference at medium frequency leading to incorrect bulk solution conductivity estimations, while the large voltage electrodes disturb the current uniformity

between two outside current collectors and, under some circumstances, produce additional low frequency load artifacts. In the four-electrode measurement, even when made by a carefully designed set-up, the contact impedance may become significant, resulting in confounding results and equivalent circuits consisting of inductive, capacitive and resistive elements related to an instrumental artifact and not to a physical condition of a studied system [24]. One therefore has to make a compromise between the effects of contact impedances, capacitive coupling between signal lines and signal lines and ground, the non-uniform current distributions, voltage drop, cable shielding, and the finite input resistance of the amplifier in considering the cells' geometric arrangements.

For a typical automotive lubricant operating at temperatures in the vicinity of 100 °C, the bulk solution resistance exceeds 1 MΩ [7]. The processes affecting the low frequency impedance features are significantly different [9] from a blocking interface reported for the Nafion membrane [20]. This paper is dedicated to determining the optimal geometrical arrangement of a cell and experimental setup for the bulk solution resistance and interfacial impedance measurements in highly resistive oil samples. For this purpose 4 two-electrode and 2 four-electrode cells with different geometries and sizes of voltage and current electrodes were fabricated.

## 2 Experimental

A schematic diagram of the two-electrode and four-electrode cells employed to examine the influence of the experimental conditions on the impedance response is shown in Fig. 1. Six sample cells consisting of symmetric grade 316 stainless steel parallel plates and rods electrodes were assembled. The electrode surfaces were initially ground with an 800 grit size abrasive disk and final polishing was performed with metal buffing rouge. Four of these cells (Cells 1–4) were two electrode symmetrical cells, with electrodes being used for both measuring voltage and supplying current.

For construction of the reference voltage electrodes in the four-electrodes cells (Cells 5–6), two additional symmetric 316 stainless steel electrodes were inserted between the two outer current-supplying electrodes. In Cell 5 the voltage electrodes were made of a fine mesh of a thickness of 0.25 mm with a geometrical area of 2 cm × 2 cm aligned exactly parallel with and covering a cross-section between the two current electrodes, with a separation gap between the voltage electrodes being 1 mm. In Cell 6 the voltage electrodes were made of a stainless steel rod with a thickness of 0.25 mm and an insertion length between the current electrodes of 1.5 cm, with a separation gap between the voltage electrodes being 1 mm.

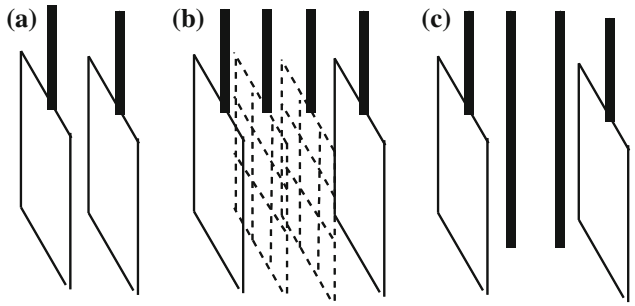


**Fig. 1** Experimental cells: **a** Cells 1–4. **b** Cell 5. **c** Cell 6

Cells 5 and 6 were also used as an equivalent substitute for Cell 1 and Cell 3, respectively, with only two outside current collectors active and the voltage electrodes disconnected from the Impedance Analyzer. That allowed studying the effect of passive elements of different area and configuration (mesh and rod) on current flow between two outside current electrodes while the homogeneity of the current flow was perturbed by the disconnected voltage electrodes. The details on exact geometry of the cells, such as visible surface area and the separation gap (distance) between the electrodes are summarized in Table 1.

All experiments were conducted in a standard 10 W-30 medium performance grade mineral oil based fresh automotive lubricant (Lubrizol Corporation, Wickliffe, OH) maintained at constant temperatures of 80 °C, 100 °C and 120 °C by a heated bath system (Lauda, Lauda-Königshofen, Germany). These temperatures were selected because they are the most representative of a typical range of operating temperatures in automotive lubricants applications. 200 mL volume glass beaker was used as a container for the sampled solutions with the electrodes exactly fitting the container.

Impedance tests were performed on an Impedance/Dielectric Analyzer (Novocontrol GmbH, Hundsangen Germany) using ZG4 cell adapter. The sampling frequencies ranged from 20 to 5 MHz with the ac perturbation of 1.5 V at equilibrium potential. All measurements were performed following an initial stabilization period to achieve better reliability of the data after large initial current variations are somewhat settled. The two-electrode cells were always shielded. The four-electrode configuration cells were used with and without active driven shielding. Plotting, analysis, and modeling of the data were performed with the WinFIT software package (Novocontrol GmbH).

## 3 Results and discussion

Impedance responses for the lubricant obtained using two-electrode Cells 1–4 and four-electrode Cells 5–6 are

**Table 1** Parameters of experimental cells

| Number of electrodes | Cell 1<br>2 | Cell 2<br>2 | Cell 3<br>2 | Cell 4<br>2 | Cell 5<br>4 | Cell 6<br>4 |
|---|---|---|---|---|---|---|
| Current electrodes | | | | | | |
| Surface area ($cm^2$) | 4.00 | 4.00 | 2.25 | 2.25 | 4.00 | 2.25 |
| Separation gap (mm) | 2.5 | 1.0 | 3.0 | 1.0 | 2.5 | 2.5 |
| Surface area/separation gap (cm) | 16 | 40 | 7.5 | 22.5 | 16 | 9 |
| Voltage electrodes | | | | | | |
| Shape | – | – | – | – | Mesh | Rod |
| Length (cm) | – | – | – | – | 2.0 | 1.5 |
| Width (cm) | – | – | – | – | 2.0 | – |
| Thickness/diameter (mm) | – | – | – | – | 0.25 | 0.25 |
| Separation gap (mm) | – | – | – | – | 1.0 | 1.0 |
| Separation gap between voltage and current electrodes (mm) | – | – | – | – | 0.5 | 0.5 |

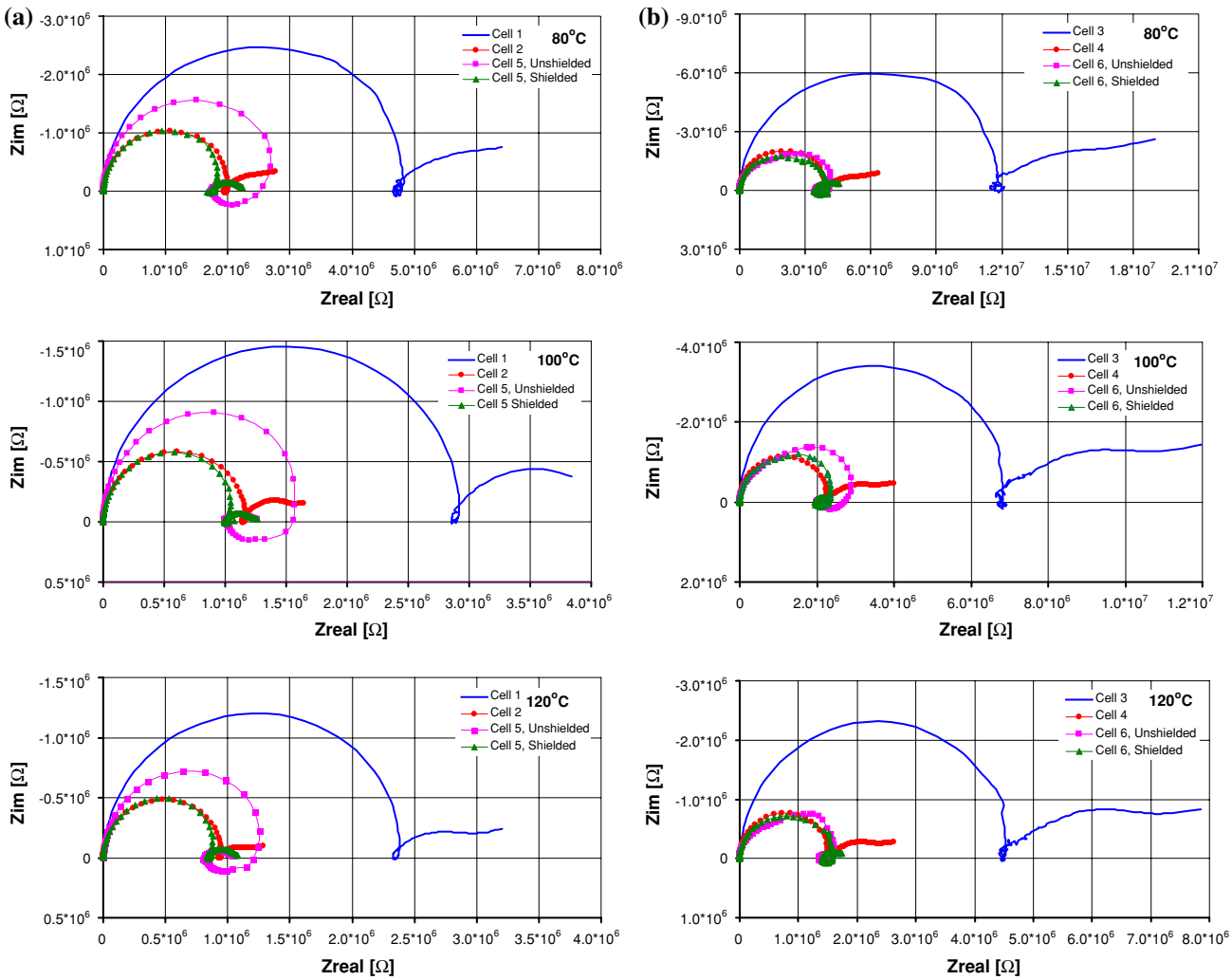


**Fig. 2** **a** Complex impedance plots of experimental data for Cell 1, Cell 2, and Cell 5. **b** Complex impedance plots of experimental data for Cell 3, Cell 4, and Cell 6

shown in Fig. 2a and b. Each plot contains four diagrams: two-electrode cell with large separation (Cell 1 or Cell 3), two-electrode cell with small separation (Cell 2 or Cell 4), four-electrode cell without activated driven shields and four-electrode cell with activated driven shields (Cell 5 or Cell 6). The data is summarized in Tables 2, 3 and 4.

A previously developed equivalent circuit model for highly resistive lubricants can be applied to the initial assessment of the data [7, 9, 15]. As in the first approximation, the high frequency segment of the impedance plot of a typical lubricant is represented by an equivalent circuit composed of a simple parallel combination of the bulk capacitance ($C_{BULK}$) and the bulk resistance ($R_{BULK}$). Tables 2, 3 and 4 demonstrate that alpha value for the bulk processes equals unity for all experiments. The lower frequency range of the EIS plot corresponds to electrochemical processes at the electrode-solution interface can be simplified and represented as a parallel combination of single interfacial charge transfer resistance ($R_{LF}$) and an interfacial capacitance ($C_{LF}$) modeled in the impedance term as a constant phase element ($CPE_{LF}$) [15].

The impedance arcs in the high-frequency region, for both cell configurations and electrodes geometries, are similar. Predictably, for two-electrode cells (Cell 1 vs. Cell 2 and Cell 3 vs. Cell 4) the increase in the surface area to gap ratio leads to a proportional decrease in the $R_{BULK}$ and $R_{LF}$ and an increase in $C_{BULK}$ and $CPE_{LF}$ values. Also the temperature effects on the two-electrode cells EIS data were in line with the previously reported trends [7], with bulk and interfacial charge transfer resistances decreasing with temperature, and the interfacial capacitance increasing (the combined $CPE_{LF}$ term is typically influenced by finite diffusion, charge transfer, and adsorption capacitance, which often increases with temperature due to the acceleration of adsorption kinetics [9]). As was shown before [7], the bulk solution capacitance is practically temperature independent. Changes in temperature and surface area to gap ratio did not cause any changes in shapes of the high

**Table 2** Experimental data at 80 °C

| | Cell 1 | Cell 2 | Cell 5 | | Cell 3 | Cell 4 | Cell 6 | |
|---|---|---|---|---|---|---|---|---|
| | | | Unshielded | Shielded | | | Unshielded | Shielded |
| $R_{BULK}$ (MΩ) | 4.90 | 2.04 | 1.80 | 1.80 | 10.27 | 4.23 | 3.40 | 3.47 |
| $C_{BULK}$ (pF) | 4.00 | 9.20 | 10.1 | 10.2 | 1.85 | 5.55 | 9.90 | 9.96 |
| Alpha 1 | 1 | 1 | 1 | 1 | 1 | 1 | 1 | 1 |
| $K_{SOL}$ (nS cm$^{-1}$) | 12.2 | 12.2 | 8.00 | 12.1 | 11.2 | 11.2 | 12.0 | 12.9 |
| $R_{LOAD}$ (kΩ) | 0 | 0 | 900 | 85.0 | 0 | 0 | 730 | 600 |
| $C_{LOAD}$ (pF) | – | – | 21.0 | 242 | – | – | 15.0 | 81.1 |
| $L_{LOAD}$ (H) | – | – | 130 | 21.7 | – | – | 2000 | 1000 |
| Alpha 2 | – | – | 1 | 1 | – | – | 1 | 1 |
| $R_{LF}$ (MΩ) | 2.66 | 1.11 | 0.390 | 0.400 | 7.05 | 2.35 | 0.830 | 0.810 |
| $C_{LF}$ (μF) | 1.43 | 3.43 | 3.80 | 3.90 | 0.42 | 1.27 | 1.61 | 1.74 |
| Alpha 3 | 0.65 | 0.65 | 0.85 | 0.83 | 0.61 | 0.63 | 0.75 | 0.75 |

**Table 3** Experimental data at 100 °C

| | Cell 1 | Cell 2 | Cell 5 | | Cell 3 | Cell 4 | Cell 6 | |
|---|---|---|---|---|---|---|---|---|
| | | | Unshielded | Shielded | | | Unshielded | Shielded |
| $R_{BULK}$ (MΩ) | 2.86 | 1.14 | 1.02 | 1.04 | 6.84 | 2.28 | 2.13 | 2.00 |
| $C_{BULK}$ (pF) | 4.27 | 10.7 | 10.8 | 10.9 | 1.86 | 5.58 | 10.4 | 11.0 |
| Alpha 1 | 1 | 1 | 1 | 1 | 1 | 1 | 1 | 1 |
| $K_{SOL}$ (nS cm$^{-1}$) | 21.5 | 21.5 | 13.7 | 21.5 | 22.0 | 22.0 | 18.2 | 20.8 |
| $R_{LOAD}$ (kΩ) | 0 | 0 | 600 | 80.0 | 0 | 0 | 500 | 80.0 |
| $C_{LOAD}$ (pF) | – | – | 21.3 | 200 | – | – | 15.0 | 81.1 |
| $L_{LOAD}$ (H) | – | – | 100 | 9.1 | – | – | 400 | 60 |
| Alpha 2 | – | – | 1 | 1 | – | – | 1 | 1 |
| $R_{LF}$ (MΩ) | 1.53 | 0.612 | 0.270 | 0.256 | 5.52 | 1.84 | 0.630 | 0.657 |
| $C_{LF}$ (μF) | 1.57 | 3.93 | 4.50 | 4.40 | 0.534 | 1.60 | 2.38 | 2.36 |
| Alpha 3 | 0.68 | 0.68 | 0.84 | 0.85 | 0.63 | 0.63 | 0.81 | 0.81 |

**Table 4** Experimental data at 120 °C

| | Cell 1 | Cell 2 | Cell 5 | | Cell 3 | Cell 4 | Cell 6 | |
|---|---|---|---|---|---|---|---|---|
| | | | Unshielded | Shielded | | | Unshielded | Shielded |
| $R_{BULK}$ (MΩ) | 2.34 | 0.936 | 0.810 | 0.830 | 4.45 | 1.48 | 1.37 | 1.39 |
| $C_{BULK}$ (pF) | 3.83 | 9.58 | 10.2 | 10.8 | 1.80 | 5.40 | 10.5 | 10.6 |
| Alpha 1 | 1 | 1 | 1 | 1 | 1 | 1 | 1 | 1 |
| $K_{SOL}$ (nS $cm^{-1}$) | 26.0 | 26.0 | 17.3 | 25.5 | 26.3 | 26.3 | 26.5 | 28.2 |
| $R_{LOAD}$ (kΩ) | 0 | 0 | 450 | 80.0 | 0 | 0 | 250 | 80.0 |
| $C_{LOAD}$ (pF) | – | – | 21.7 | 205 | – | – | 10.5 | 100 |
| $L_{LOAD}$ (H) | – | – | 45 | 9.8 | – | – | 200 | 50 |
| Alpha 2 | – | – | 1 | 1 | – | – | 1 | 1 |
| $R_{LF}$ (MΩ) | 0.714 | 0.286 | 0.210 | 0.213 | 3.10 | 1.03 | 0.432 | 0.434 |
| $C_{LF}$ (μF) | 1.94 | 4.85 | 5.22 | 5.43 | 0.690 | 2.07 | 3.38 | 3.58 |
| Alpha 3 | 0.68 | 0.68 | 0.87 | 0.87 | 0.64 | 0.64 | 0.83 | 0.85 |

and low frequency sections of complex impedance plots, demonstrating that no changes in the processes controlling the impedance response occurred.

When Cell 5 and Cell 6 were used as two-electrode cells by disconnecting the internal voltage electrodes and using the outside electrodes both as source of current and for voltage measurement, small inductive loops at the border of the bulk and interfacial regions were observed. These features are likely due to the breaking up of homogeneity of the current flow between two outside current electrodes by the disconnected internal electrodes, which are still present, sitting passively between the two outside current/voltage electrodes. This effect is more noticeable for Cell 5 which employs mesh voltage electrodes with large surface area as the effect of interference is larger than for Cell 6 equipped with smaller surface area rod-shaped voltage electrodes. Therefore the current flow in Cell 5 is much less homogeneous than in Cell 6.

When the four-electrode Cells (5 and 6) were tested, some significant changes due to the removal of the interfacial effects on the voltage electrodes were observed. The low frequency interfacial region became much better defined as a single process represented by a parallel resistance-capacitance combination. It should be noted that the two-electrode experiments (Cells 1–4) clearly revealed at least two processes in the studied low frequency impedance region—a semicircular shaped adsorption region at the higher frequencies and what appeared to be the diffusion region at very low frequencies, similar to what was reported before [9]. For the two-electrode cells, build-up of a layer of non surface-active species electrostatically attracted to the interface impedes the mass-transport process of the surface-active molecules to the electrode surface. These surface-active species are attempting to chemically adsorb on the surface, but have to be transported through a layer of non-surface-active species in the vicinity of the electrode-solution interface. The non-surface-active species are attracted there through excessive polarization, but have insufficient ability to exchange their respective charges with the electrode unless operated at large dc overvoltages and submilliHertz frequencies [9].

When the four-electrode Cells 5 and 6 were introduced, only one well-resolved semicircular impedance feature was observed at the low frequency. The low frequency resistances decreased by 2–4 times, the capacitance increased, and the alpha parameters became closer to unity, when compared to experiments conducted under the same temperature and other conditions in Cells 2 and 4, respectively. Temperature effects were essentially the same as for the two-electrode cells. Very little difference in low frequency impedance features were observed between shielded and unshielded arrangements in Cells 5 and Cell 6 (Tables 2, 3 and 4).

The interfacial effects are not measured in the four-electrode cells, contrary to the explanation offered in [20], and this type of low frequency impedance behavior was interpreted for certain temperature conditions (and the related sample conductivity values) as being caused by a geometric artifact introduced through the voltage electrodes with larger relative thicknesses [22]. The depression in the low frequency semicircle was explained by a transmission line effect along the electrode strip width due to the differences in the local electric field distribution at different frequencies caused by the mainly capacitive blocking nature of the voltage electrodes. Since the thickness of the voltage electrodes is not zero, a part of the lubricant solution is shorted by the metal of well-conducting voltage electrodes behaving as bipolar electrodes. At low frequencies the voltage is measured between the centerlines, while at high frequencies the voltage is measured between the inner edges of the voltage electrodes. The resulting maximum error for an electrode with

a rectangular cross-section should be equal to the ratio of the width of the electrodes and the distance between the center lines of the electrodes. In the case of both Cell 5 and Cell 6 that gives an approximate error of ~20%, which is essentially equal to the ratio of the respective resistance values $R_{LF}$ and ($R_{LF} + R_{BULK}$) (Tables 2, 3, 4). It would be interesting to note that for the studied temperature range this error is consistently ~1–2% lower in Cell 6 where the rounded surface of the rod-like voltage electrodes probably provided less of a contrasting difference in a local spatial voltage distribution than the rectangular surface of the voltage electrodes in Cell 5. We will dedicate our future studies to investigating this phenomenon.

For the same experimental conditions, bulk solution impedance characteristics for Cell 5 and Cell 6 are close to the values for the Cell 2 and Cell 4, respectively, as the separation distances between the respective voltage electrodes and surface areas of current electrodes are the same for these cells. The high frequency impedance parameters for the four-electrode cells have slightly lower $R_{BULK}$ and higher $C_{BULK}$ than for the two-electrode cells, probably due to the fact that the voltage electrodes in Cells 5 and 6 short a part of the conducting path through the lubricant solution. However, a very large inductive-resistive-capacitive distortion appears in the medium-frequency range (1000–1 Hz), in particular for Cell 6 with its smaller voltage electrodes, a higher solution resistance (80 °C), and without activated shields. The appearance of this distortion leads to a large deviation in the medium-frequency region, from where conductivity data are usually derived.

Due to the medium-frequency distortion, extracting conductivity data by fitting only the larger arcs or using the medium-frequency imaginary maximum ($Z_{IM(MAX)}$) often leads to erroneous results. Tables 2, 3 and 4 present a comparison of the bulk solution conductivity $K_{SOL}$ values calculated using different experimental cells by simple interpolation of the $Z_{IM(MAX)}$ value of the high frequency semicircle to a low frequency imaginary minimum. This analysis yields the estimations of $R_{BULK}$ and from that the solution conductivity values using the formula combining the values of the gap, $l$, between the voltage electrodes and the surface area of the current electrodes, $A$:

$$K_{SOL} = \frac{l}{2Z_{IM(MAX)}A} \quad (1)$$

The data in Table 1 demonstrate that when conductivity values are being extracted from the data obtained using the four-electrode cell configuration, the medium frequency inductive-resistive-capacitive distortion interference results in conductivity measurement errors of up to 40% for Cell 5, and up to 15% for the Cell 6. Previous studies also reported [20] this type of phenomenon, which lead to recommendation of using voltage electrodes with smaller surface area/separation gap ratio for more accurate measurements of bulk solution conductivity. However, when the driven shields were applied, the conductivity measurement error in Cell 5 decreased to ~1–2%, while the conductivity measurement error in Cell 6 decreased to only 5–10%, making the cell with voltage electrodes with larger surface area/separation gap ratio significantly more accurate as the effects of the inductive-resistive-capacitive distortion were better mitigated.

A schematic diagram of the impedance equivalent circuits for the two- and four-electrode electrochemical cells is shown in Fig. 3. For the two-electrode cells the lubricant bulk solution is represented by a bulk resistance, $R_{BULK}$, and bulk capacitance, $C_{BULK}$, connected in parallel. Parallel combination of $R_{CT}$, and $CPE_{DL}$, and series absorption and diffusion impedances, represents the interfacial low frequency impedance (Fig. 3a).

In the four-electrode cells, the voltage-sensing electrodes are separated from the current injectors, and due to the high input impedance of the voltage measuring circuit, negligible current passes through them. The effect of the interfacial charge build up is not measured, and the bulk solution equivalent circuit remains as a single $R_{BULK}|C_{BULK}$ parallel circuit. The low frequency impedance of the four-electrode cells, which essentially represents the geometric artifact described above, can be represented by a parallel combination of resistance $R_{LF}$ and capacitance $C_{LF}$, both of which have no physical meaning but reflect the geometry of the sampling cell (Fig. 3b). The additional impedance in the medium frequency originated from loading artifact related to the experimental conditions and cell arrangements [22–28]. The medium frequency portion of the circuit can be modeled as a parallel combination of loading resistance $R_{LOAD}$, inductance $L_{LOAD}$, and capacitance $C_{LOAD}$. The resulting equations describing the

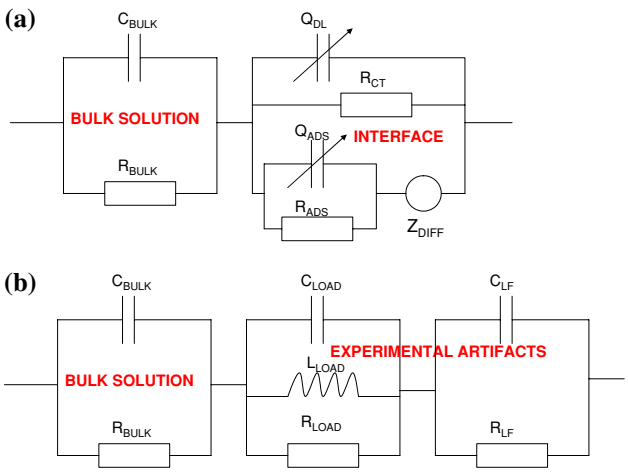


**Fig. 3** Evolution of the EC diagram from **a** the two-electrode Cell to **b** the four-electrode Cell

corresponding impedance of the total four-electrode cells become:

$$Z_{\mathrm{REAL}} = \frac{R_{\mathrm{BULK}}}{1+\omega^2 R_{\mathrm{BULK}}^2 C_{\mathrm{BULK}}^2} + \frac{\omega^2 R_{\mathrm{LOAD}} L_{\mathrm{LOAD}}^2}{R_{\mathrm{LOAD}}^2 (1-\omega^2 L_{\mathrm{LOAD}} C_{\mathrm{LOAD}})^2 + \omega^2 L_{\mathrm{LOAD}}^2} + \frac{R_{\mathrm{LF}}}{1+\omega^2 R_{\mathrm{LF}}^2 C_{\mathrm{LF}}^2} \quad (2)$$

$$Z_{\mathrm{IM}} = -j\frac{\omega R_{\mathrm{BULK}}^2 C_{\mathrm{BULK}}}{1+\omega^2 R_{\mathrm{BULK}}^2 C_{\mathrm{BULK}}^2} + j\frac{\omega R_{\mathrm{LOAD}}^2 L_{\mathrm{LOAD}} (1-\omega^2 L_{\mathrm{LOAD}} C_{\mathrm{LOAD}})}{R_{\mathrm{LOAD}}^2 (1-\omega^2 L_{\mathrm{LOAD}} C_{\mathrm{LOAD}})^2 + \omega^2 L_{\mathrm{LOAD}}^2} - j\frac{\omega R_{\mathrm{LF}}^2 C_{\mathrm{LF}}}{1+\omega^2 R_{\mathrm{LF}}^2 C_{\mathrm{LF}}^2} \quad (3)$$

The simulated data corresponding to these equations is presented in Fig. 4.

It is likely that $R_{\mathrm{LOAD}}$ and $C_{\mathrm{LOAD}}$ are related to contact resistance of the voltage electrodes circuit, which includes the electrodes and the cables (shielded or not shielded). Both values are in fact positive, resulting in a positive corresponding time constant $\tau = R_{\mathrm{LOAD}}\, C_{\mathrm{LOAD}}$ and hence are not in violation of the Kramers-Kronig transformation rules [24]. The capacitance is most prominent at high frequencies of ~10 MHz–10 kHz, resistance at medium frequencies ~1 kHz, and at lower frequencies the inductance plays a predominant role in the loading portion of the total impedance of the sample. Inductive load is most noticeable as it causes a large shift in the imaginary impedance of the sample at frequency range of 1000–10 Hz. Resistance of the load causes increase and peaking of the total real impedance at 100–10 kHz range (Fig. 4).

Table 1 demonstrates that Cell 6, with smaller surface area voltage electrodes, has consistently lower $R_{\mathrm{LOAD}}$ values than Cell 5. The capacitive loads in both Cell 5 and Cell 6 are approximately the same, and probably are related to the combined loading of the apparatus (open-circuit) and unshielded cables [26], which are ~100 pF m$^{-1}$. A total load of ~20 pF is expected for the ~20 cm long, non-shielded cables used in these experiments. The inductive loads are significantly higher in the Cell 6 arrangement. When the active shielding was introduced, the distortion and corresponding impedances at medium frequencies decreased significantly, especially for Cell 5 when large voltage electrodes were operating at higher temperatures. Higher temperatures lead to a decrease in the contact resistance [27] resulting in a smaller loading artifact. Introduction of the active shielding resulted in decreasing of the overall $R_{\mathrm{LOAD}}|C_{\mathrm{LOAD}}|L_{\mathrm{LOAD}}$ loading by ~10 times for Cell 5, and by ~2–4 times for Cell 6. The differences in loading reductions by shielded cables between Cell 5 and Cell 6 are particularly large at lower temperatures where often little to no decrease in the $R_{\mathrm{LOAD}}|C_{\mathrm{LOAD}}|L_{\mathrm{LOAD}}$ loading in Cell 6 was observed (Fig. 4). Below we will describe the reason for appearance of the inductive loading in this circuit due to a voltage divider effect related to gradual increase in the loading impedances of the voltage electrodes with decrease in the frequency, and resulting decrease of an actual measured voltage drop across the analyzed sample.

As Fig. 5 illustrates, the measured impedance of the system depends purely on the properties and impedance of the material between the two voltage electrodes ($Z_{\mathrm{SAMPLE}}$). Two voltage-measuring reference electrodes connected through a high impedance device (so that negligible current flows across these interfaces) are placed in the electrochemical cell between counter and working electrodes. When the active shields are used, for the equipment employed in this testing the input impedance of both voltage electrodes $Z_{\mathrm{INPUT}}$ consists of the capacitance $C_{\mathrm{INPUT}}$ with a value of ~10 pF in parallel with resistance $R_{\mathrm{INPUT}}$ with a value of ~$10^{12}$ Ω. Except for very high impedance samples, $R_{\mathrm{INPUT}}$ can usually be neglected, and the input impedance at the terminals becomes:

$$Z_{\mathrm{INPUT}} = \frac{R_{\mathrm{INPUT}}}{1+j\omega R_{\mathrm{INPUT}} C_{\mathrm{INPUT}}} \sim \frac{1}{j\omega C_{\mathrm{INPUT}}} \quad (4)$$

or approximately 160 MΩ at a frequency of 100 Hz.

The four-electrode experimental arrangement allows the contact impedance of two symmetrical current-generating electrodes ($Z_C$) to be eliminated from the impedance spectrum. The magnitude of the contact impedances of the voltage electrodes ($Z_R$) was estimated from a two-electrode impedance measurement using only the two internal voltage electrodes—2 cm × 2 cm meshes in Cell 5 and 1.5 cm × 0.25 mm rods in Cell 6. Low frequency impedance features at the corresponding complex impedance plots were analyzed to approximate the contact impedances of these electrodes. It was modeled as a parallel combination of $R_{\mathrm{R}}$ and $CPE_{\mathrm{R}}$, and from the experimentally obtained parameters such as: CPE coefficient Q, circular frequency $\omega_{\mathrm{MAX}}$—corresponding to the maximum value $Z_{\mathrm{IM}}(\omega_{\mathrm{MAX}})$, and the α-parameter, an effective equivalent capacitance $C_R$ can be estimated:

$$C_R = Q\omega_{\mathrm{MAX}}^{\alpha-1} \quad (5)$$

producing experimental values on the order of ~$10^{-7}$ F. This can then be used in Eq. 6 for estimating magnitude of the contact impedances of voltage electrodes $Z_R$ for all frequencies:

$$Z_R = \frac{R_R}{1+j\omega R_R C_R} \quad (6)$$

As the voltage reference points $V_{\mathrm{HIGH}}$ and $V_{\mathrm{LOW}}$ are non-zero, $Z_{\mathrm{INPUT}}$ load on both voltage electrodes causes parasitic currents to flow. This parasitic current flows out

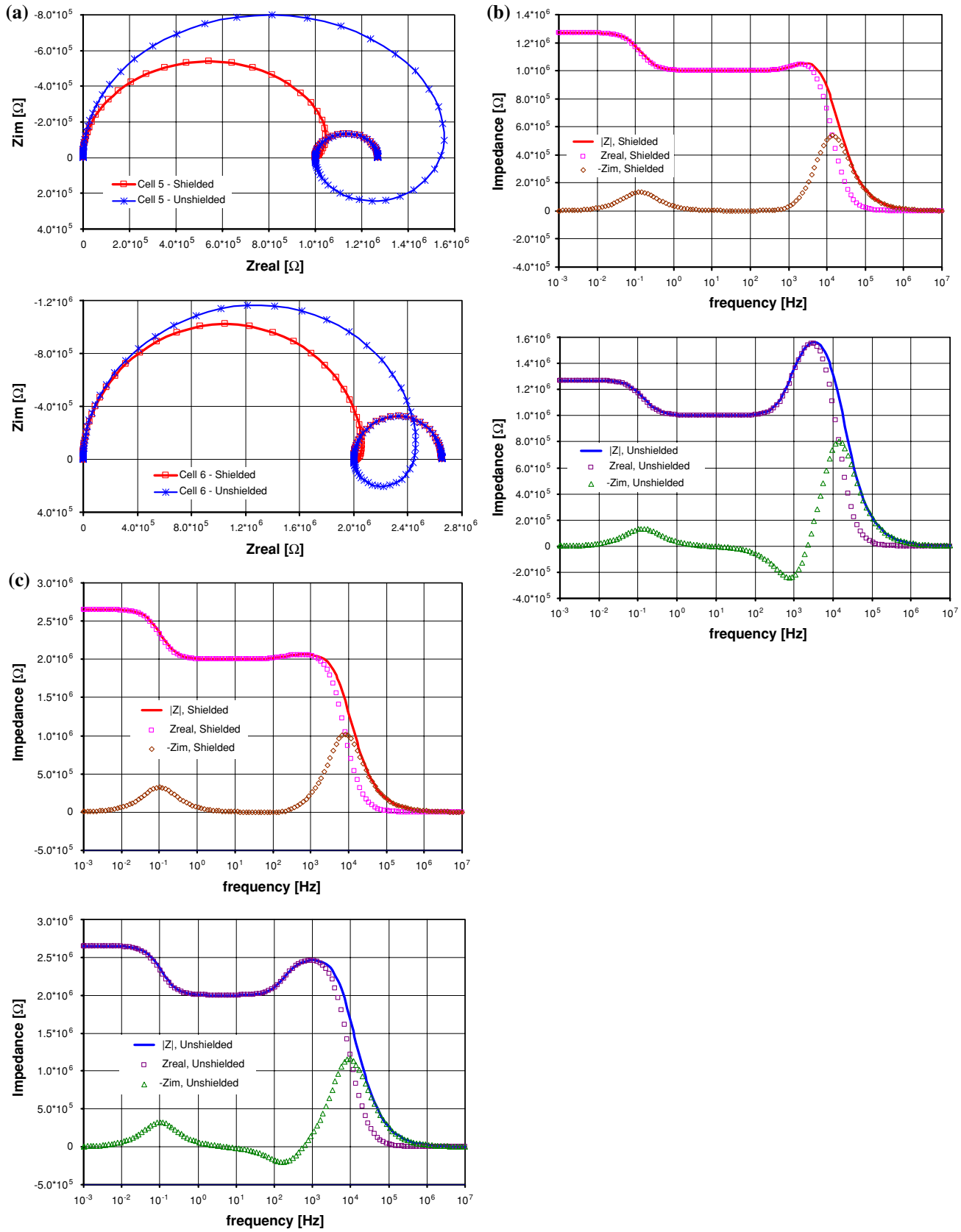


**Fig. 4** **a** Complex impedance plots of shielded vs. non-shielded cables for Cell 5 and Cell 6 at 100 °C. **b** Bode plots of shielded vs. non-shielded cables for Cell 5 at 100 °C. **c** Bode plots of shielded vs. non-shielded cables for Cell 6 at 100 °C

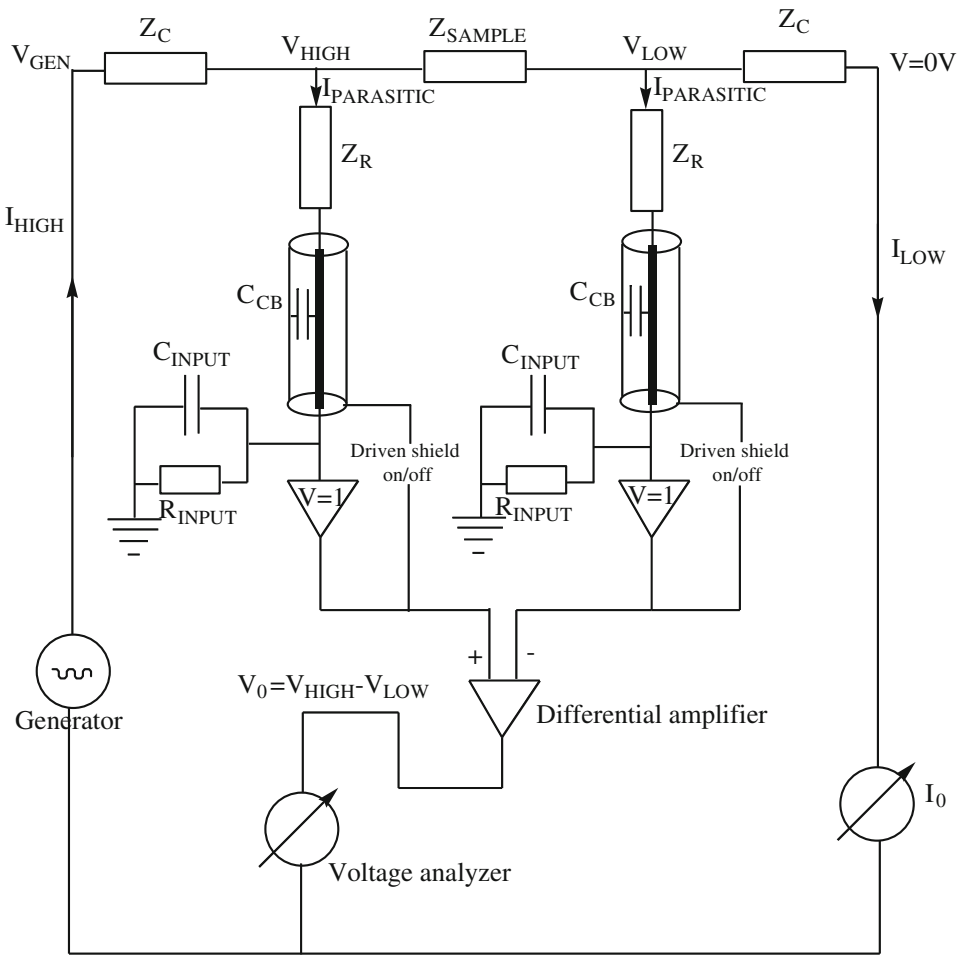


**Fig. 5** Four-electrode measurement schematic

from the sample, which usually creates a small error in the total sample current measurement. That error can be neglected as long as $Z_{\mathrm{INPUT}} \gg Z_{\mathrm{SAMPLE}}$. Sample current becomes therefore:

$$I_{\mathrm{SAMPLE}} = \frac{V_{\mathrm{HIGH}} - V_{\mathrm{LOW}}}{Z_{\mathrm{SAMPLE}}} - I_{\mathrm{PARASITIC}} \tag{7}$$

At the same time the parasitic current passing through the contact impedance causes the voltage divider effect [27], leading to an increase in the voltage drop across the contact impedance as:

$$V_R = I_{\mathrm{PARASITIC}} Z_R \tag{8}$$

This voltage drop creates an error in the measured voltages $V_{\mathrm{HIGH}}$ and $V_{\mathrm{LOW}}$. With decrease in sampling frequency $\omega$, $Z_R$ increases according to Eq. 6 leading to increase in $V_R$ and decrease in $V_{\mathrm{SAMPLE}}$ as:

$$V_{\mathrm{SAMPLE}} = V_{\mathrm{HIGH}} - V_{\mathrm{LOW}} - V_R = V_O - V_R \tag{9}$$

This effect in fact leads to a situation where the measured sample impedance $Z_{\mathrm{MEASURED}}$ decreases, and the inductive loading rises, in the medium-frequency range. Inductive medium frequency load has no physical meaning; however, it reflects the property of the sample cell with the type of four-electrode measurement and not an error introduced by the instrumentation. Therefore, in addition to the need to suppress parasitic current $I_{\mathrm{PARASITIC}}$ and to keep $I_{\mathrm{PARASITIC}} \ll I_{\mathrm{SAMPLE}}$ one has to make sure that $V_R$ is small compared against measured total voltage difference $V_0 = V_{\mathrm{HIGH}} - V_{\mathrm{LOW}}$. For this purpose a voltage electrode configuration with $Z_R \ll Z_{\mathrm{SAMPLE}}$ should be chosen. This again requires a large electrode area for the voltage electrodes. This can be largely accomplished by the use of two flat metal mesh electrodes mounted in between the two outer electrodes (such as in Cell 5); and placing each of the voltage electrodes as close to the two outer current electrodes as possible. Thus, measured sample impedance can be expressed considering all the above corrections as:

$$Z_{\mathrm{MEASURED}} = V_{\mathrm{SAMPLE}} / I_{\mathrm{SAMPLE}} \tag{10}$$

Measured sample resistance between points $V_{\mathrm{HIGH}}$ and $V_{\mathrm{LOW}}$ from the circuit (Fig. 5), considering input impedances $Z_{\mathrm{INPUT}}$ and contact impedances of the voltage electrodes $Z_R$ is:

$$\frac{1}{Z_{\text{MEASURED}}} = \frac{1}{Z_{\text{SAMPLE}}} + \frac{1}{2Z_R + 2Z_{\text{INPUT}}} \tag{11}$$

and:

$$Z_{\text{MEASURED}} = Z_{\text{SAMPLE}} \frac{2Z_{\text{INPUT}} + 2Z_R}{2Z_{\text{INPUT}} + 2Z_R + Z_{\text{SAMPLE}}} \tag{12}$$

As indicated above, for the optimal measurement the condition should exist so $Z_R \ll Z_{\text{SAMPLE}} \ll Z_{\text{INPUT}}$. For a given sample that can be achieved by choosing an electrode configuration which creates relatively small sample impedance by increasing the electrode area and minimizing the spacing between two voltages electrodes, paying a preferential attention to keeping $Z_{\text{SAMPLE}} \ll Z_{\text{INPUT}}$. If this is done, the equation reduces to:

$$Z_{\text{MEASURED}} \approx Z_{\text{SAMPLE}} \tag{13}$$

For the samples with high resistance, such as the system studied here, the difference between $Z_{\text{INPUT}}$ and $Z_{\text{MEASURED}}$ is minimal at high frequencies (Fig. 6) leading to a possibility of a substantial systematic high frequency error. This type of effect has been reported in the literature [26].

An additional consideration calls for minimization of the interference of the voltage electrodes to the homogeneity of the current flow between the two outside current electrodes by using electrodes with a small surface area and minimum interference (such as our Cell 6). As mentioned above, this arrangement may in fact be preferred when only bulk solution estimation from high frequency measurement is required.

The voltage electrode cable capacity and the leakage resistance from the signal line to the grounded shield are loads for signal sources with large source impedance. As can be seen from the schematics, the capacity of the voltage electrode cables, $C_{\text{CB}}$, are in parallel to the input capacitance, $C_{\text{INPUT}}$, if the outer cable shield is connected to ground (driven shields off). Therefore, the input impedance, $Z_{\text{INPUT}}$, can be more broadly defined as a combination of the cable capacitance and insulation resistance with the input capacitance and resistance of the amplifier circuit. The capacity of a standard BNC cable is about 100 pF $m^{-1}$ and therefore can significantly increase the total voltage input capacity as $C_{\text{CB}} = L_{\text{CB}} * 100$ pF $m^{-1}$ where $L_{\text{CB}}$ is the length of the cable. In that case the total input impedance becomes smaller as:

$$Z_{\text{INPUT}} = \frac{R_{\text{INPUT}}}{1 + \omega R_{\text{INPUT}}(C_{\text{INPUT}} + C_{\text{CB}})} \tag{14}$$

That introduces a change in Eq. 12, and also increases the parasitic current $I_{\text{PARASITIC}}$ determined from the total input impedance. The result leads to larger values for the voltage drop across the contact impedance, Eq. 8, and therefore decreases the real sample voltage and measured sample impedance. As such, total inductive loading increases, as was observed in our experimental data (Fig. 3).

The analysis of experimental data using Eqs. 4–14 shows that at some medium frequency there is max error in $V_{\text{SAMPLE}}$ which translates to the error in impedance measurement $Z_{\text{SAMPLE}}$. The error when the shielded cables were used is ~3 times lower than in non-shielded (Voltage 2.5 vs. 7.5%, impedance 1.7 vs. 5.2%—Fig. 7).

Using shorter cables and optimizing the geometry of the voltage electrodes remain the simplest physical solutions to minimizing the measurement errors. Unfortunately circumstances do not always permit changing the physical properties of the electrochemical cell; therefore, active driven shielding must be used. Active shielding is

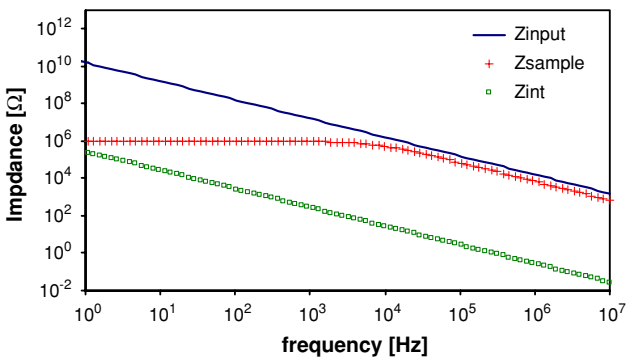


**Fig. 6** $Z_{\text{INPUT}}$, $Z_{\text{SAMPLE}}$, and $Z_{\text{INT}}$ vs. Frequency

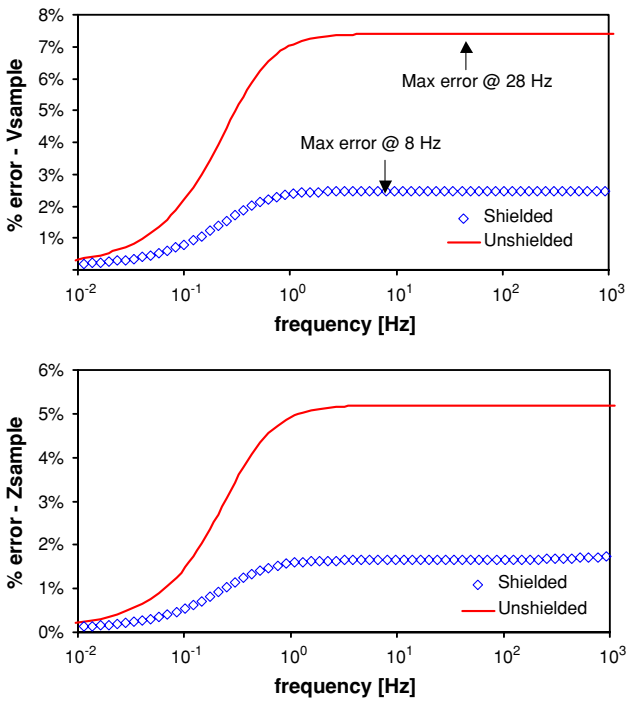


**Fig. 7** Calculated $V_{\text{SAMPLE}}$ error and $Z_{\text{SAMPLE}}$ error versus frequency in the medium frequency (1000–0.01 Hz) range

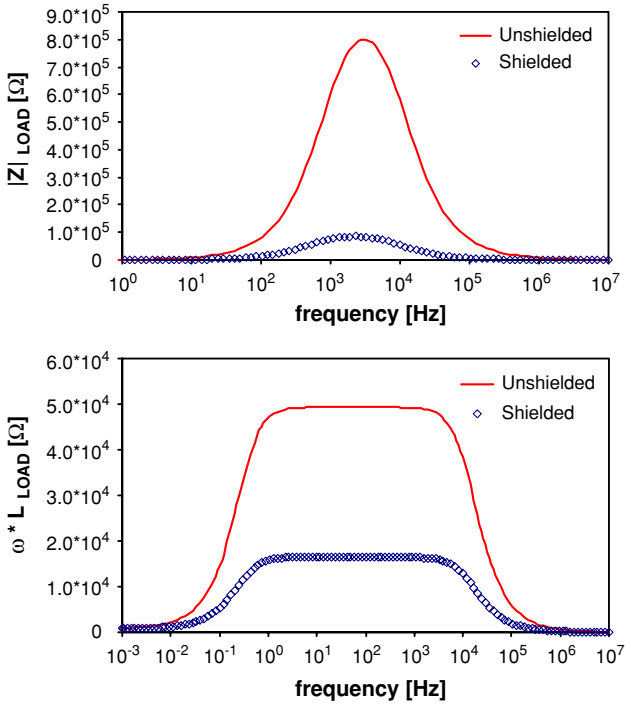


**Fig. 8** Total impedance and Inductive impedance in four-electrode cells using shielded and non-shielded cables with Cell 5

accomplished by surrounding the cables with a screen that is at the same potential as the signal lead. By connecting the shield to the input amplifier voltage output, the shield is kept at the same potential as the electrode. In principle the cable capacity is still present using this setup, but the active shielding rejects the capacitive current [22] and minimizes the effects of the amplifier open-circuit parasitic capacitance by an order of magnitude [26]. With the shielding engaged the total input parasitic current is reduced to the current related to high impedance of the input amplifier $Z_{\mathrm{INPUT}}$. Thus, the sole source of interfacial loads will be the input capacitance of the amplifier circuit.

In practice, this concept works only partly. It is necessary to extend the active shield on the leads as close as possible to the sample. This prevents the leads to the current electrodes from affecting other signal lines due to stray capacitance. Experimentally, driven shields reduced the combined effect of the cable and amplifier open circuit capacitance and resulting inductive and total medium frequency impedance loading by a factor 3–10 at frequencies below 10 kHz (Fig. 8), in agreement with our experimental data (Fig. 4).

## 4 Conclusion

Complex impedance plots obtained using four-electrode cells are more strongly influenced by cell geometry and experimental conditions than are two-electrode cells. The four-electrode cells offer an advantage of excluding the interfacial effects from the measurement; however, achieving "minimal error measurement" configuration depends on a number of experimental and instrumentation parameters that often point in opposite directions, and therefore is almost impossible to achieve. A complex impedance response is observed in a four-electrode cell revealing two features with no real physical meaning—an inductive arc due to a voltage divider effect in the medium-frequency regime, and additional capacitive load caused by geometry and separation gap of the voltage electrodes in the low frequency. In contrast, two-electrode cells provide simple and well-defined impedance spectra from which the impedance data can readily be extracted.

The four-electrode cell impedance measurements are reliable if the sample impedance $Z_{\mathrm{SAMPLE}}$ is sufficiently small with respect to the input impedance $Z_{\mathrm{INPUT}}$, which requires high conductivity/low bulk solution resistance of the sample, elevated solution temperature, reduction of the influence of the cables impedance through shorter leads and active shielding, selection of an instrument with very high input impedance, and voltage electrodes with a small separation gap and large surface areas. If only a bulk solution conductivity measurement by extrapolation of higher frequency Zim values to the point of Zim $\rightarrow$ 0 is required, the smaller voltage electrodes can be used. Reducing the electrodes surface area/separation gap ratio facilitates deconvolution of bulk impedance from the lower frequency interfacial impedances for data obtained from either two-electrode or four-electrode cells.

For more accurate characterization of the system and better mitigation of the inductive and capacitive loadings of the circuit of the voltage electrodes at medium and low frequencies, the large surface area meshes should be used for voltage electrodes in conjunction with the active shields. Choosing finer grade meshes for these electrodes is a way to expand the available surface area; however, the tradeoff will be increased electric field inhomogeneity.

Smaller values of the input impedance $Z_{\mathrm{INPUT}}$ lead to inductive artifacts. The interface impedances of current electrodes $Z_C$ and of voltage electrodes $Z_R$ should be very low to minimize the voltage divider effect, and to not cause a substantial interruption in the current flow from the outside current electrodes; while the thickness of the voltage electrodes should be kept to a minimum with respect to the distance between these electrodes to minimize the low frequency transmission line geometric effect. These conditions lead to the complicated requirements for shape and surface area properties of the voltage electrodes. Additionally, a careful and difficult analysis of several contributions, such as: solution resistance, positioning of the electrodes, geometry of the electrodes, and active

shielding becomes necessary. However, even with using perfect instrumentation and experimental arrangements, measurements will not be completely artifacts-free.

## References


1. Hanai T (1968) In: Sherman P (ed) Emulsion science, Chap 5. Academic Press, London, p 353
2. Dukhin S (1971) Dielectric properties of disperse systems. In: Mitijevic E (ed) Surface and colloid science. Wiley Science, New York, pp 83–165
3. Wang SS, Lee HS (1997) Sens Actuators B 40:193–197
4. MacDonald JR (1987) Impedance spectroscopy. Wiley, New York
5. Grimnes S, Martinsen OG (2000) Bioimpedance and bioelectricity basics. Academic Press, London
6. Krause S (2001) In: Bard AJ (ed) Encyclopedia of electrochemistry, vol 3 Impedance methods, vol 3. Wiley-VCH, Weinheim
7. Lvovich VF, Smiechowski MF (2006) Electrochim Acta 51:1487–1496
8. Lvovich VF, Skursha DB, Boyle FP (2005) Method for on-line monitoring of quality and condition of non-aqueous fluids. US Patent 6,861,851
9. Lvovich VF, Smiechowski MF (2008) Electrochim Acta 53:7375–7385
10. Smiechowski MF, Lvovich VF (2002) J Electroanal Chem 534:171–180
11. Smiechowski MF, Lvovich VF (2005) J Electroanal Chem 577:67–78
12. Goodlive SA, Lvovich VF, Humphrey BK, Boyle FP (2004) SAE technical paper series SAE 2004-01-3010
13. Boyle FP, Lvovich VF, Leye H (2005) In: Proceedings of the 2005 annual meeting Society of Tribologists and Lubrication Engineers, Las Vegas, 16 May 2005
14. Smiechowski MF, Lvovich VF (2003) Sens Actuators B 96:261–267
15. Lvovich VF, Smiechowski MF, Liu CC (2006) Sens Actuators B 119:490–496
16. Han DG, Choi GM (1999) Electrochim Acta 44:4155–4161
17. Asami K (1995) Evaluation of colloids by dielectric spectroscopy, HP Application Note 380-3, p 1
18. Jakoby B, Vellekoop MJ (2004) Physical sensors for water-in-oil emulsions. Sens Actuators A 110:28–32
19. Kornbrekke RE, Morrison ID, Oja T (1992) Langmuir 8:1211–1217
20. Xie Z, Song C, Andreaus B, Navessin T, Shi Z, Zhang J, Holdcroft S (2006) J Electrochem Soc 153(10):E173–E178
21. Cahan BD, Wainright JS (1993) J Electrochem Soc 140(12): L185–L186
22. Fafilek G (2005) Solid State Ionics 176(25–28):2023–2029
23. Fafilek G, Breiter MW (1997) J Electroanal Chem 430:269–278
24. Vanýsek P (2005) In: Artifacts and their manifestation in impedance measurements. Presentation at 207th meeting of the Electrochemical Society, Quebec City, Canada, 15–20 May 2005
25. Boukamp B (2001) Solid State Ionics 143(1):47–55
26. Edwards DD, Hwang J-H, Ford SJ, Mason TO (1997) Solid State Ionics 99:85–93
27. Hsieh G, Ford SJ, Mason TO, Pederson LR (1996) Solid State Ionics 91:191–201
28. Fletcher S (2001) Electrochem Commun 3:692–696